

Narrow-linewidth red-emission Eu³⁺-doped TiO₂ spheres for light-emitting diodes

Peifen Zhu, Hongyang Zhu, Weiping Qin, Breno H. Dantas, Wei Sun, Chee-Keong Tan, and Nelson Tansu

Citation: *Journal of Applied Physics* **119**, 124305 (2016); doi: 10.1063/1.4944944

View online: <http://dx.doi.org/10.1063/1.4944944>

View Table of Contents: <http://scitation.aip.org/content/aip/journal/jap/119/12?ver=pdfcov>

Published by the [AIP Publishing](#)

Articles you may be interested in

Investigation of Eu–Mn energy transfer in $A_3MgSi_2O_8 : Eu^{2+}, Mn^{2+}$ ($A = Ca, Sr, Ba$) for light-emitting diodes for plant cultivation

Appl. Phys. Lett. **93**, 144101 (2008); 10.1063/1.2996256

Near-ultraviolet excitable orange-yellow $Sr_3(Al_2O_5)Cl_2 : Eu^{2+}$ phosphor for potential application in light-emitting diodes

Appl. Phys. Lett. **93**, 131114 (2008); 10.1063/1.2996278

One-step preparation of $Ca-\alpha-SiAlON : Eu^{2+}$ fine powder phosphors for white light-emitting diodes

Appl. Phys. Lett. **92**, 191904 (2008); 10.1063/1.2920209

Thermally stable luminescence of $KSrPO_4 : Eu^{2+}$ phosphor for white light UV light-emitting diodes

Appl. Phys. Lett. **90**, 151108 (2007); 10.1063/1.2721846

White light-emitting diodes of GaN-based $Sr_2SiO_4 : Eu$ and the luminescent properties

Appl. Phys. Lett. **82**, 683 (2003); 10.1063/1.1544055



NEW Special Topic Sections

NOW ONLINE
Lithium Niobate Properties and Applications:
Reviews of Emerging Trends

AIP | Applied Physics Reviews

Narrow-linewidth red-emission Eu^{3+} -doped TiO_2 spheres for light-emitting diodes

Peifen Zhu,^{1,2,a)} Hongyang Zhu,³ Weiping Qin,^{4,b)} Breno H. Dantas,¹ Wei Sun,¹ Chee-Keong Tan,¹ and Nelson Tansu^{1,c)}

¹Center for Photonics and Nanoelectronics, Department of Electrical and Computer Engineering, Lehigh University, Bethlehem, Pennsylvania 18015, USA

²Department of Physics and Engineering Physics, The University of Tulsa, Tulsa, Oklahoma 74104, USA

³State Key Laboratory of Superhard Materials, Jilin University, Changchun, Jilin 130012, China

⁴State Key Laboratory on Integrated Optoelectronics, College of Electronic Science and Engineering, Jilin University, Changchun, Jilin 130012, China

(Received 20 November 2015; accepted 16 March 2016; published online 29 March 2016)

In this work, the amorphous Eu^{3+} -doped TiO_2 spheres were synthesized by low cost mixed-solvent method, while the anatase and rutile spheres can be obtained by annealing the as-synthesized amorphous TiO_2 spheres at elevated temperatures. The optical properties of Eu^{3+} -doped TiO_2 spheres were also investigated, and strong red emission (centered at 610 nm) with narrow line-width of 30 nm was observed under 465 nm or 394 nm excitations for the Eu^{3+} -doped anatase TiO_2 spheres. Our findings indicate the potential of using Eu^{3+} -doped TiO_2 spheres to achieve red emission with InGaN blue light emitting diodes (LEDs). Owing to the high light extraction efficiency in the GaN-based LEDs using anatase TiO_2 spheres as demonstrated in our previous works, this work shows the strong potential of Eu^{3+} -doped TiO_2 spheres as the red phosphor material for high efficiency GaN-based white light-emitting diode. © 2016 AIP Publishing LLC.

[<http://dx.doi.org/10.1063/1.4944944>]

I. INTRODUCTION

GaN-based light-emitting diodes (LEDs) have been rapidly developing for modern lighting and display technology due to their superior efficiency.¹ High-efficiency InGaN blue LEDs have been realized in recent decades,^{2–9} which are attributed to the substantial improvement in the material growth, the internal quantum efficiency, and the light extraction efficiency. In recent years, significant efforts have also been devoted to addressing the efficiency-droop issue^{10–16} and optimizing the light extraction efficiency in the InGaN LED devices.^{17–27} These advances have resulted in the continuous improvement in the InGaN LEDs performance, allowing the lower energy consumption for higher lumens output.

The development of the high efficiency blue LEDs, coupled with the advances in the yellow phosphor materials, has directly resulted in the revolution of white light technology.²⁸ Specially, the approach of coating the yellow phosphor material (YAG: Ce^{3+}) on the InGaN blue LEDs has been widely implemented due to the advantage of low-cost, high efficiency, and high temperature stability. However, the high color correlated temperature (CCT \sim 6000 K) and the low red color rendering index (CRI $<$ 75) in the yellow phosphor converted InGaN white LEDs are undesirable for indoor lighting applications (CCT $<$ 4000 K and CRI $>$ 80). There are several different methods that can be used to achieve the white light emission with potentially desirable CCT and CRI features, which include the use of (a) red,

green, and blue (RGB) multichip LED, (b) multi-emitting-centers single phosphor with blue InGaN LED, and (c) multi-phosphors with blue InGaN LED.²⁸

The white LED based on the RGB multichip approach provides high color rendering index and high chromaticity stability, but extending the nitride-based LED devices towards longer wavelength especially in the red spectral regime has been found to be difficult due to the fundamental phase separation issue in the high In-content InGaN quantum well (QW) layer.²⁹ Several approaches have been proposed to achieve red emission including InGaN-delta-InN QW,³⁰ Eu-doped GaN QW instead of InGaN QW,³¹ InGaN with AlGaN interlayer QW,³² and Type-II InGaN-GaNAs QW.³³ However, these approaches have yet to be practically implemented for white light LED technology due to the high fabrication cost.

In comparison to the RGB multichip approach, the multi-emitting-centers single phosphor and multi-phosphors methods are potentially low-cost method, which are similar to the conventional phosphor method. For the case of multi-emitting-centers single phosphor method, additional red-emitting centers are introduced into the YAG: Ce^{3+} lattice to compensate the red spectral deficiency of YAG: Ce^{3+} . For the case of multi-phosphors method, a variety of blue, green, yellow, and red emitting phosphor can be chosen and mixed together. While both methods can produce warm-white light with sufficiently high CRI values (80–98), the multi-phosphors method provides additional flexibility in developing new phosphors to produce the white light emission from the InGaN blue LED with high CRI and CCT characteristics. Thus, finding the suitable phosphor especially the red emitting phosphor to couple with the yellow phosphor is critical

^{a)}Email: peifen-zhu@utulsa.edu

^{b)}Email: wpqin@jlu.edu.cn

^{c)}Email: tansu@lehigh.edu

towards generating white light emission from the LEDs. The key for the red phosphor is to obtain high quantum yield material with emission in the red color ($\lambda \sim 620$ nm) while having narrow full width at half maximum (FWHM) (~ 30 nm).

Recently, TiO₂ material has been suggested as a promising phosphor host material due to the advantages of low cost, high transparency in the visible light region, good thermal, chemical, and mechanical properties. Our recent findings showed that the TiO₂ sphere array with anatase phase placed on top of the GaN-based thin film flip chip (TFFC) LEDs leads to optimum light extraction efficiency as compared to the TiO₂ sphere array with different phases, attributed to the refractive index matching with the GaN material.²⁴ Our results showed that the optimized extraction efficiency of 86% could be achieved for the TFFC LEDs by using anatase TiO₂ microlens arrays.²⁶ In addition, our previous works had also demonstrated that the deposition of TiO₂ sphere arrays on top of the LEDs can be carried out through rapid convective deposition method, which is a low-cost, easily implemented, and wafer-scale method.^{21–24} Most recently, Eu³⁺-doped TiO₂ material is suggested to be the promising red phosphor due to the transparency in the visible spectral regime. These developments indicate that the implementation of Eu³⁺-doped TiO₂ spheres as phosphor material will potentially provide a much needed red emission from blue InGaN LED with high light extraction efficiency, which will be important for the white LED technology.

However, the TiO₂ spheres with high quality are not commercially available, and obtaining monodisperse homogeneous TiO₂ spheres is challenging due to the critical growth condition.^{34–36} Specifically, the high hydrolysis rate of Titania precursor during the synthesis process leads to the non-uniformity of TiO₂ sphere size,³⁴ resulting in the light extraction efficiency reduction of LED with TiO₂ sphere arrays. Therefore, the optimization of TiO₂ sphere growth condition to obtain the monodisperse TiO₂ spheres and Eu-doped TiO₂ spheres is important for achieving red emission with high light extraction efficiency for the blue InGaN LED.

In this work, the synthesis of the Eu³⁺-doped TiO₂ spheres is carried out through mixed-solvent method and the optical properties of the spheres are investigated. The growth conditions of the TiO₂ spheres were optimized taking into account the effects of ammonia, the ratio of acetonitrile to acetone in the mixed solvents, and the concentration of titanium tetrabutoxide (TBOT). The phase transformation condition was also investigated by the thermal annealing process, in which the amorphous TiO₂ were transferred to the anatase TiO₂ and rutile TiO₂. Our photoluminescence (PL) measurement shows peak emission at 610 nm (red) under the light excitation of 465 nm (blue) and 394 nm (violet) for the Eu³⁺-doped TiO₂ spheres. Our study suggests the strong potential of applying Eu³⁺-doped TiO₂ spheres in high efficiency white LEDs.

II. SYNTHESIS OF Eu³⁺-DOPED TiO₂ SPHERES

Recently, mixed-solvent method has been developed into an effective method to obtain monodisperse spherical particles, such as CeO₂ and CdS.^{37,38} Adjusting the ratio of

mixed solvents not only can slow down the hydrolysis rate but also can control the diffusion rate of the precursors, both of which have significant effect on the morphology of the particles. In the synthesis of TiO₂ spheres via mixed solvent method, the TBOT was used as the precursor and the ammonia served as the catalyst. The ethanol and acetonitrile were used as the solvent in the process. All the reactants were used without further purification. In order to investigate the effect of ammonia on the morphology of TiO₂ spheres, two samples of TiO₂ particles were prepared in the ethanol solvent with and without ammonia, respectively. Also, to investigate the effect of acetonitrile on the formation of TiO₂ particles, we adjusted the ratio of acetonitrile to ethanol. As a typical synthesis, two solutions were prepared by mixing acetonitrile and ethanol with different ratios. The mixed solution was then stirred for 30 min. Next, an amount of ammonia and TBOT were added to the two solutions, respectively. After substantial stirring, the two solutions were mixed and stirred for 2 h. The obtained products were centrifuged and washed with absolute ethanol for 4 times. Afterwards, the samples were dried at 80 °C for 12 h.

Figures 1(a) and 1(b) show the scanning electron micrograph (SEM) images of TiO₂ particles prepared in the ethanol without and with ammonia, respectively. Note that the concentration of the chemicals except the ammonia in each reaction was the same. Without the addition of the ammonia, the irregular TiO₂ particles were obtained as shown in Figure 1(a). However, when the distilled water was substituted by the ammonia, more spherical particles can be formed as shown in Figure 1(b). This finding indicated that the NH₃·H₂O played a very important role in forming the spherical particles. In the process, the ammonia was decomposed into ammonium (NH₄⁺) and hydroxide (OH⁻); thus, the NH₄⁺ overcame repulsive barrier and drew the negatively charged ≡TiO⁻ together. The formation mechanism of TiO₂ spheres is illustrated in Figure 2. The NH₄⁺ is firstly absorbed by the negatively charged ≡TiO⁻ forming the cores of the particle. Afterwards, the ≡TiO⁻ migrates to the core and starts the condensation process. Therefore, the ammonia contributes to the formation of spherical TiO₂ particles.

Though the spherical particles were formed under the assistance of ammonia, the particles tended to stick together as shown in Figure 1(b), due to the high solubility of TBOT and its hydrolysates. Note that the hydrolysis of TBOT molecules will result in the coexistence of TBOT and its hydrolysates in the solution. Due to the high solubility of TBOT and its hydrolysates in the ethanol, the interaction between the solute and the solvent molecules was significant leading to the unseparated spherical particle aggregate. In contrast, the solubility of TBOT and its hydrolysates is relatively lower in the acetonitrile as the solvent. As a result, when a certain amount of acetonitrile is added to the ethanol solution, the interactions between solutes (TBOT and its hydrolysates) and solvents (ethanol and acetonitrile) became weaker. Therefore, the TBOT can easily diffuse onto the surface of hydrolysates and then hydrolyze and condense under the catalysis of NH₄⁺ to form monodisperse spherical TiO₂ particles. This means that the optimized diffusion process for

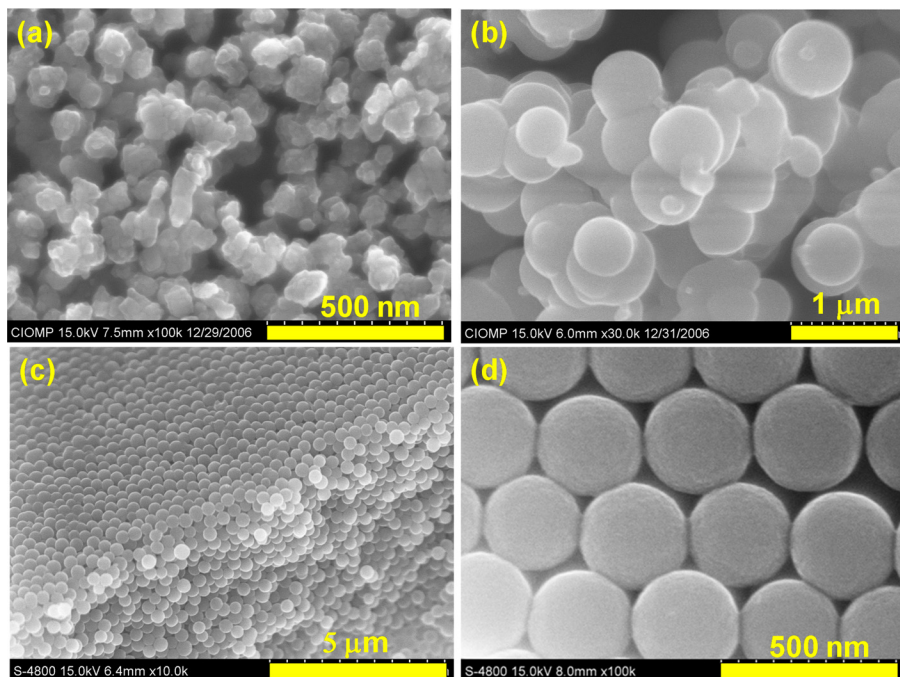


FIG. 1. SEM images of TiO₂ particles synthesized under the different conditions: (a) without ammonia and acetonitrile, (b) with ammonia but without acetonitrile, and (c) with ammonia and acetonitrile (the inset is an enlarged image).

TBOT and its hydrolysates can be achieved by adjusting the ratio of ethanol to acetonitrile. Figures 1(c) and 1(d) show the SEM images of the monodisperse TiO₂ spheres obtained using the 3:1 ratio of ethanol to acetonitrile.

The size of TiO₂ particles depends on the concentration of TBOT in the mixed solvent. Note that the hydrolysis rate is one of the key factors determining the size of TiO₂ particles as faster hydrolysis rate yields larger TiO₂ particles.^{34–36} By reducing the TBOT concentration,³⁶ the hydrolysis rate decreases leading to smaller TiO₂ particles. In addition, the reaction temperature has significant effect on the particle size. High reaction temperature promotes hydrolysis of TBOT and then increases the number of titania nuclei. As a result, the size decreases with decreased reaction

temperature.³⁹ This explains why the reaction happens at ambient temperature.

The structure of TiO₂ particles was analyzed by X-ray diffraction (XRD) (Rigaku D/max-2000 X-ray powder diffractometer) using Cu K α radiation ($\lambda = 1.54178 \text{ \AA}$). The overall images and sizes of the particles were characterized by field emission scanning electron microscopy (SEM, S-4800). The excitation and emission spectra were measured by fluorescence spectrometers (Hitachi F-4500 and F-2700).

Figure 3 presents the XRD patterns for the TiO₂ samples with 300-nm diameter before and after annealing at various temperatures (350 °C, 500 °C, 650 °C, and 850 °C) for 2 h. The as-prepared sample did not show any diffraction peaks, indicating that the as-synthesized TiO₂ spheres are amorphous. No

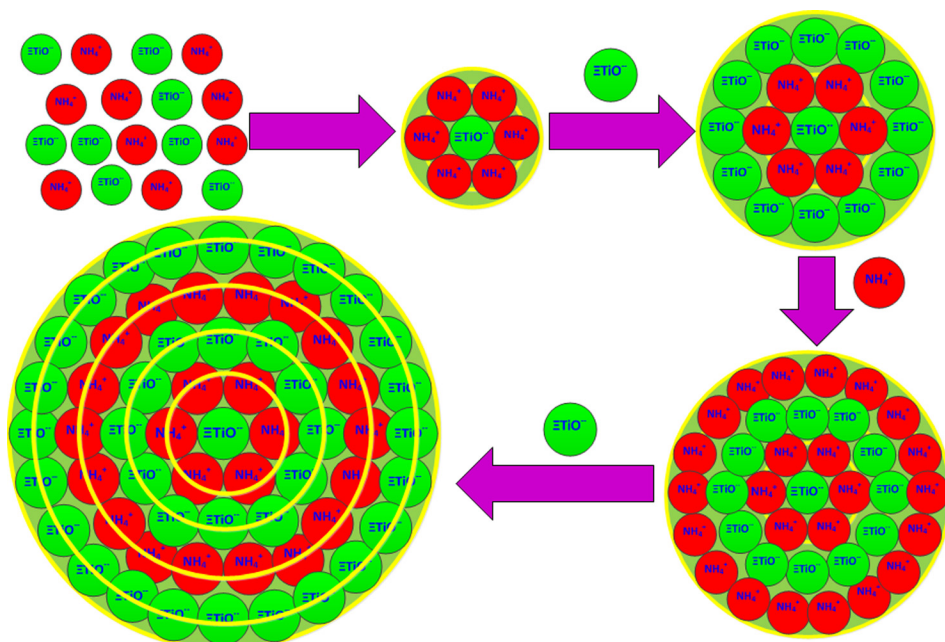


FIG. 2. Schematics of sphere formation process.

peak was observed for the sample annealed at 350 °C indicating that no phase transformation occurs. Several diffraction peaks appeared for the sample annealed at 500 °C, which implies the phase transforming from amorphous to anatase phase of TiO₂ (JCPDS 21-1272). No other phase pattern for rutile or brookite TiO₂ could be found at this temperature. When the annealing temperature increased to 800 °C, all the diffraction peaks correspond to the rutile phase of TiO₂ (JCPDS 21-1276). From the XRD patterns, the sample annealed at 650 °C consists of both anatase and rutile phases, as diffraction peaks of both phases were observed at this annealing temperature.

As the monodisperse TiO₂ spheres can be obtained by using the mixed-solvent method, the Eu³⁺-doped TiO₂ spheres could be synthesized in the similar manner. In our study, the Eu³⁺-doped TiO₂ spheres were prepared as following: two identical solutions were prepared by mixing acetonitrile and ethanol. The mixed solution was stirred for 30 min. Then a specific amount of ammonia was added to one of the two solutions, and Eu(NO₃)₃ and TBOT were added to the other solution. Note that the concentration of the Eu³⁺ in the Eu³⁺-doped TiO₂ spheres can be determined by calculating the ratio of Eu(NO₃)₃ and TBOT in the synthesis. In other words, the quantities of the Eu(NO₃)₃ and TBOT that need to be added in the synthesis can be calculated by using the following equations:

$$n_{TBOT}(mol) = C_{TBOT} \left(\frac{mol}{L} \right) \times V_{TBOT}(L), \quad (1)$$

$$m_{Eu(NO_3)_3 \times 6H_2O}(g) = 446 \left(\frac{g}{mol} \right) \times n_{TBOT}(mol) \times Q\%, \quad (2)$$

where n_{TBOT} is the quantity of Titanium (IV) n-Butoxide in the unit of mol. The concentration C_{TBOT} ($\frac{mol}{L}$ or molar) used in Equation (1) is generally labeled on the bottle of the substance and $V_{TBOT}(L)$ is the volume of TBOT solution added in the reaction. The molar mass of the Eu(NO₃)₃ hexahydrate is given by 446 ($\frac{g}{mol}$) and the Q% represents the percentage desired to be used in the reaction. Note that the percentage (Q% of Eu³⁺-doped TiO₂) indicated in the experiment represents the molar mass ratios of Eu(NO₃)₃ and TBOT used in the synthesis of the nanomaterials. After substantial stirring

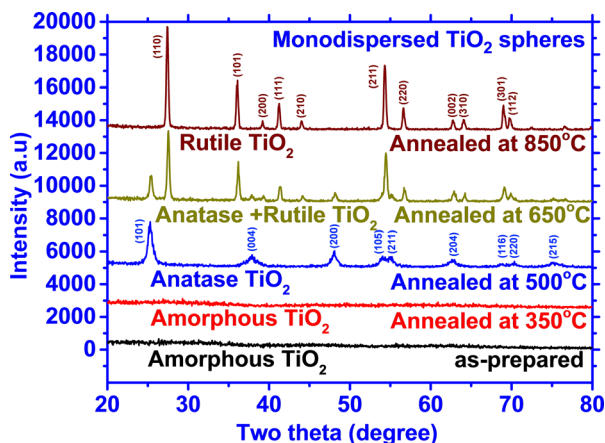


FIG. 3. XRD patterns of undoped TiO₂ at different annealing temperatures.

for half an hour, these two solutions were mixed and stirred for another 2 h. The obtained products were centrifuged and washed with absolute ethanol for 4 times, and then dried at 80 °C for 12 h. Afterwards, the as-prepared Eu³⁺-doped TiO₂ particles were annealed at 350 °C, 500 °C, 650 °C, and 850 °C for 2 h, respectively.

III. OPTICAL PROPERTIES AND THEIR POTENTIAL APPLICATION IN WHITE LEDs

Figure 4 shows the PL excitation spectrum corresponding to the 611 nm emission of Eu³⁺ doped TiO₂. The spectra exhibit several sharp peaks owing to the Eu³⁺ f → f transition and a broad excitation band with a maximum at 270 nm. Tsuboi and co-workers observed two broad excitation bands in Eu³⁺ doped TiO₂ nanoparticles at around 320 nm and 270 nm.^{21,22} The 320 nm excitation band is the same as the absorption band observed in non-doped TiO₂. Therefore, the 320 nm band was attributed to the band-to-band transition in the host lattice while the 270 nm band corresponds to the charge transfer (CT) band from the 2p orbital of O²⁻ ligands to the 4f orbital of Eu³⁺ ion. Zeng and coworkers also measured the excitation of Eu³⁺-doped TiO₂ nanotube and concluded that the peak at 275 nm is attributed to the charge transfer between Eu³⁺ and O²⁻ and the excitation peak at 312 nm is attributed to the energy transfer from the TiO₂ nanotube matrix to Eu³⁺ ions.⁴⁰ In our experiment, only the 270 nm band was observed. There are two possibilities: it is either CT band or the absorption band of TiO₂.

The clarification of the origin for this 270 nm broad band absorption can be done by performing the excitation and PL measurement for the undoped TiO₂ spheres annealed at 350 °C, 500 °C, 650 °C, and 850 °C as shown in Figure 5. The PL spectrum under 270 nm excitation exhibits a broad ultraviolet emission band centered at 380 nm with FWHM of about 69 nm [see Figure 5(a)], which is attributed to electron transition from the conduction band (CB) to the valence band (VB). For the PL excitation (PLE) spectra monitoring 380 nm emission, a broad excitation band with peak at 270 nm was observed [see Figure 5(b)]. Therefore, the 270 nm broad band in Eu³⁺-doped TiO₂ is attributed to the

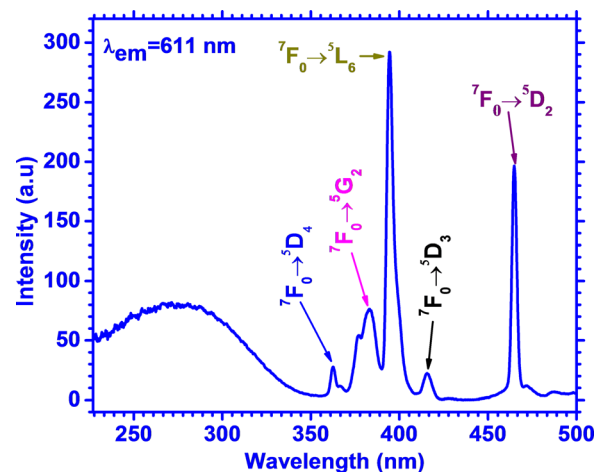


FIG. 4. The excitation spectrum of Eu³⁺-doped amorphous TiO₂ spheres monitoring 610 nm emission.

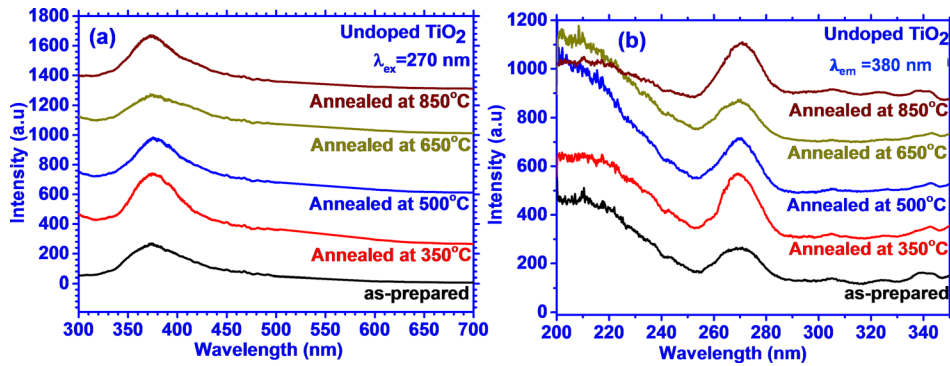


FIG. 5. (a) The emission spectra of TiO₂ spheres under 270 nm excitation and (b) the excitation band spectra corresponding for 380 nm emission wavelength.

absorption of TiO₂. When the TiO₂ is excited by the UV light, the excitation energy absorbed by TiO₂ promotes the electrons from VB to CB. Some of the electrons are excited from the valence band and then trapped to the defect states. Through the non-radiative decay process, the electrons in the defect states recombine with the holes in the VB resulting in the UV emission. Compared to the reported TiO₂ crystals,^{41–43} the TiO₂ spheres synthesized in this work yield a larger band gap, which is consistent with the results from Pan and coworkers.⁴⁴ The larger band gap observed in our study is attributed to the amorphous phase of the TiO₂ particles,⁴⁵ as indicated in the XRD patterns. Thus, the 270 nm broad band absorption most possibly originates from the undoped TiO₂ spheres. Note that the CT band between the O²⁻ and Eu³⁺ will result in 275 nm peak in the PLE spectra,⁴⁰ leading to overlapping between the CT band and the 270 nm broadband absorption from the un-doped TiO₂ spheres. Thus, the CT band between the O²⁻ and Eu³⁺ could not be observed in the PLE spectrum. This result suggested that Eu³⁺ emission is associated with an energy transfer process from the TiO₂ to the Eu³⁺.

More information about the energy transfer between TiO₂ and Eu³⁺ can be obtained by the investigation of the emission spectra of TiO₂ doped with various molar ratio concentrations Q% of Eu³⁺. The PL spectrum with 270 nm excitation for the samples with Eu³⁺ molar ratio concentration Q% = 0%, 1%, 10%, and 15% is shown in Figure 6(a), respectively. For the purpose of comparison, the spectrum is normalized by 380 nm emission. Compared to the un-doped TiO₂ spheres, five emission peaks at 576, 590, 611, 649, and 697 nm can be observed as the Eu³⁺ molar ratio concentration increased. These 5 different peaks correspond to the Eu³⁺ transition from ⁵D₀ to ⁷F_J (J = 0, 1, 2, 3, 4), respectively.⁴⁶ These peaks show strong

inhomogeneous broadening, which is attributed to the distribution of the Eu³⁺ in the amorphous titania region and also the larger ionic radius of Eu³⁺ (0.098 nm) compared to that of Ti⁴⁺ (0.068 nm).⁴⁷ Figure 6(b) shows that the integrated emission intensity centered at 610 nm increased with the increase of the Eu³⁺ molar ratio concentration. The transition of Eu³⁺ centered at 610 nm is lower than that of TiO₂ peaking at 380 nm at relatively lower Eu³⁺ molar ratio concentration (Q% = 1%), which is reversed by increasing the Eu³⁺ molar ratio concentration. This implies the energy transfer process between the TiO₂ and Eu³⁺ that has been proved by Tachikawa *et al.*⁴⁸ Our findings are consistent with the conclusion obtained by Zeng *et al.*⁴⁹ that the emission from ⁵D₀ to ⁷F_J (J = 0, 1, 2, 3, 4) of Eu³⁺ ion increased with the increase of Eu³⁺ content in Eu³⁺-doped TiO₂ particles.

Figures 7(a) and 7(b) show PL spectra of Eu³⁺-doped TiO₂ particles with 394 nm excitation and 465 nm excitation, respectively. As shown in Figures 7(a) and 7(b), there is a strong emission peak at 610 nm (red) for Eu³⁺-doped TiO₂ spheres under the excitation light of either 394 nm (violet) or 465 nm (blue). This indicates a strong potential of using GaN blue LED to obtain the red light emission in the 610 nm regime by applying the Eu³⁺-doped TiO₂ spheres. In addition, the emission intensity under the excitation of 394 nm and 465 nm increased with the increase in Eu³⁺ molar ratio concentration, which is attributed to the increased luminescent center in the TiO₂ matrix.

Figure 8 illustrated the PL investigation of the Eu³⁺-doped TiO₂ particles with various annealing temperatures. The emission spectra of 10% Eu³⁺-doped TiO₂ at various annealing temperatures are shown in Figure 8(a). The emission intensity peaking at 610 nm varies accordingly with the annealing temperature. Specifically, the maximum intensity

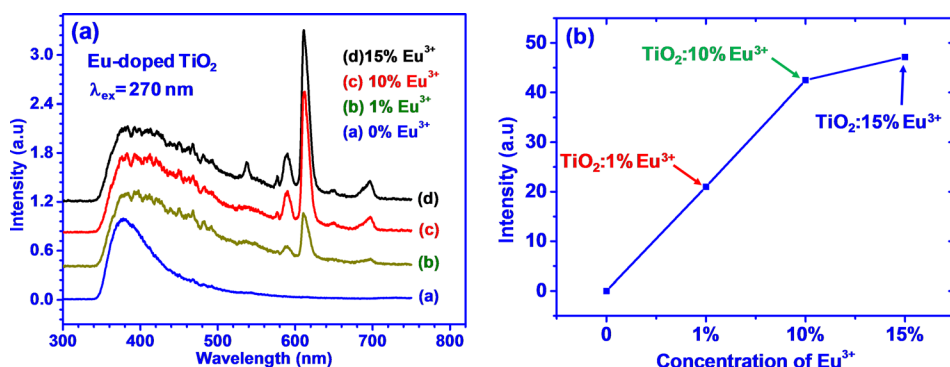


FIG. 6. (a) The emission (normalized by 380 nm emission) spectra of Eu³⁺-doped TiO₂ spheres with various Eu³⁺ molar ratio concentrations under 270 nm excitation and (b) integrated intensity of emission centered at 610 nm for Eu³⁺-doped TiO₂ spheres with various molar ratio concentrations.

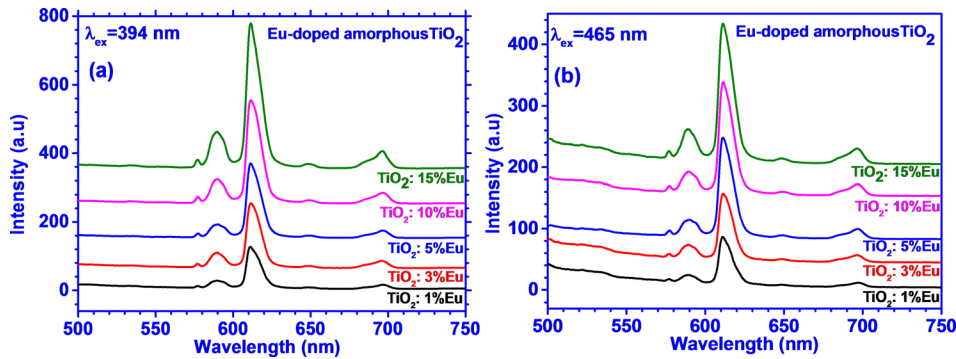


FIG. 7. (a) The emission spectra of Eu^{3+} -doped TiO_2 spheres with various Eu^{3+} molar ratio concentrations under 394 nm excitation and (b) the emission spectra of Eu^{3+} -doped TiO_2 spheres with various Eu^{3+} molar ratio concentrations under 465 nm excitation.

can be observed for Eu^{3+} -doped TiO_2 particles annealed at 500 °C. Further increase in the annealing temperature leads to the reduction of the emission intensity peaking at 610 nm. Note that the emission intensity for the Eu^{3+} -doped TiO_2 spheres annealed at 350 °C is also smaller than that of Eu^{3+} -doped TiO_2 spheres annealed at 500 °C. This indicates that the anatase Eu^{3+} -doped TiO_2 spheres (annealed at 500 °C) provide the highest red light conversion intensity from 465 nm blue light excitation, as compared to the amorphous and rutile Eu^{3+} -doped TiO_2 spheres.

Figure 8(b) shows the excitation spectra of Eu^{3+} -doped TiO_2 sphere with molar ratio concentration $Q = 10\%$ at various annealing temperatures. As shown in Figure 8(b), both the 394 nm and 465 nm absorption peaks exist for the as-prepared sample and samples with low annealing temperature (<750 °C). However, only the 465 nm absorption peak could be observed when the annealing temperature increased up to 750 °C and beyond. This phenomenon observed in our PL measurement for the samples annealed at high temperature is likely attributed to the phase changes in the sphere structures. When the Eu^{3+} -doped TiO_2 spheres are annealed at high temperature of 900 °C, the phase is transformed from amorphous to rutile structure, resulting in the modification in

the luminescent properties of the spheres. Specifically, the intensity of absorption centered at 465 nm initially increased with increased annealing temperature and then the maximum intensity was observed for the sample annealed at temperature of 500 °C, which corresponds to the anatase phase of TiO_2 . The intensity then started to decrease with further increase in temperature. Figure 8(c) shows the normalized excitation spectra for the 10% Eu^{3+} -doped TiO_2 spheres annealed at different temperatures. By normalizing the excitation spectra with respect to the 465 nm absorption peak, obvious trend can be observed that only 465 nm peak will exist when temperature increased beyond 500 °C.

For further understanding on how the Eu^{3+} concentration affects the red emission property of the Eu^{3+} -doped TiO_2 spheres, we performed an experiment with higher molar ratio percentage (Q) of $\text{Eu}(\text{NO}_3)_3$ and TBOT. The comparison was performed for samples with Q -ratios of 75% and 10% following the same synthesis procedure. Afterwards, the samples were annealed at various temperatures and then characterized by PL measurement with Hitachi F2700. Figures 9(a) and 9(b) show the emission spectra of Eu^{3+} -doped TiO_2 spheres with $Q = 10\%$ and $Q = 75\%$ Eu^{3+} concentration under 465 nm excitation, respectively. Comparing these two figures,

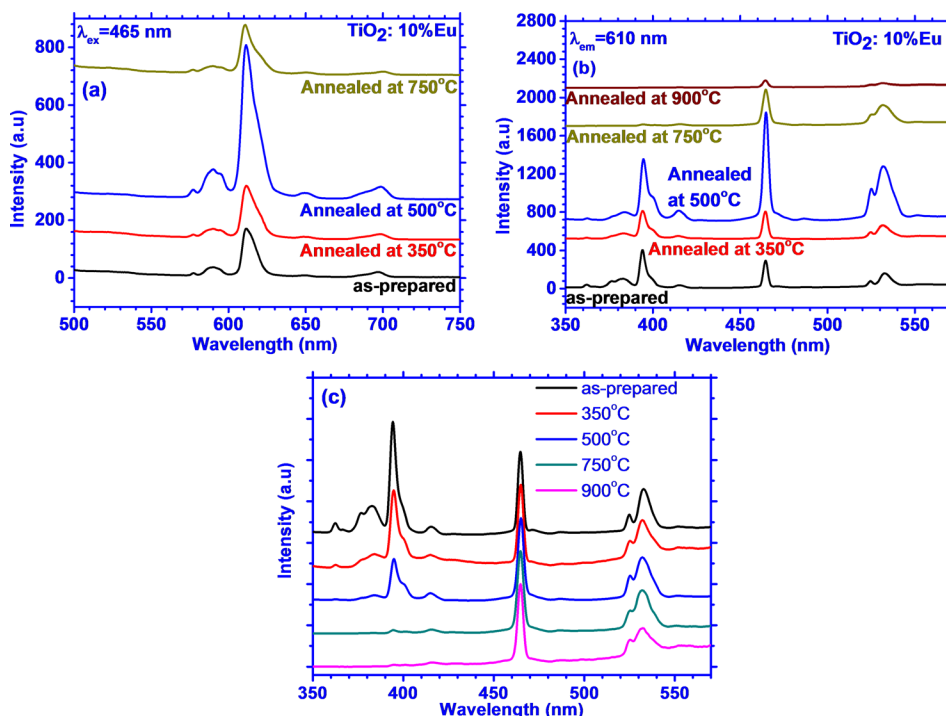


FIG. 8. (a) The emission spectra of 10% Eu^{3+} -doped TiO_2 spheres annealed at various temperatures under 465 nm excitation. (b) The excitation spectra of 10% Eu^{3+} -doped TiO_2 spheres annealed at different temperatures monitoring 610 nm emission. (c) The normalized excitation spectra Eu^{3+} -doped TiO_2 spheres annealed at different temperatures monitoring 610 nm emission.

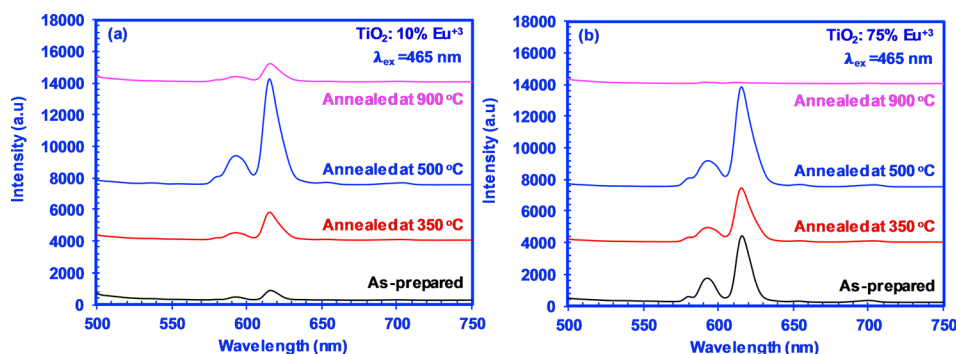


FIG. 9. (a) The emission spectra of Eu^{3+} -doped TiO_2 spheres with 10% Eu^{3+} molar ratio concentrations under 270 nm excitation and (b) the emission spectra of Eu^{3+} -doped TiO_2 spheres with 75% Eu^{3+} molar ratio concentrations under 270 nm excitation.

the Eu^{3+} -doped TiO_2 spheres with $Q=75\%$ annealed at low temperature ($<500^\circ\text{C}$) show higher emission intensity compared to that of the Eu^{3+} -doped TiO_2 spheres with $Q=10\%$. However, when the annealing temperature increased beyond 500°C , the peak emission intensity of the Eu^{3+} -doped TiO_2 spheres with $Q=75\%$ becomes lower than that of Eu^{3+} -doped TiO_2 spheres with $Q=10\%$. Eventually, the sample with 75% Eu^{3+} molar ratio concentration yields almost zero emission when the annealing temperature reaches 900°C , while the Eu^{3+} -doped TiO_2 spheres with 10% Eu^{3+} molar ratio concentration still have relatively small peak emission. This phenomenon suggests that the annealing temperature optimization should be performed with respect to different Eu^{3+} concentrations of the Eu^{3+} -doped TiO_2 spheres to achieve the optimized red emission property for potential applications. The use of lower Eu^{3+} -doped TiO_2 sphere can be more practical, but the difference in the optical response of the higher Eu^{3+} -doped TiO_2 spheres as a function of annealing temperature has scientific merit. Note that the difference in molar ratio concentration of dopant in the TiO_2 spheres shows significant differences in the properties with annealing temperature, which will be the topic of interest for future optimization studies of these nanomaterials.

It is important to note that our study at the moment is focused in optimizing the synthesis of Eu^{3+} -doped TiO_2 spheres and demonstrating the potential of using Eu^{3+} -doped TiO_2 spheres for blue or ultraviolet light converting into red light emission. Note that the light extraction efficiency has been shown to increase significantly by using the LEDs with TiO_2 sphere arrays.²⁴ This indicates the potential of Eu^{3+} -doped TiO_2 spheres in enhancing the emission efficiency. However, the research in the Eu^{3+} -doped TiO_2 spheres is still in the early development stage and further studies will be required to investigate the emission efficiency of the Eu^{3+} -doped TiO_2 spheres, which will be important for practical device implementation.

IV. CONCLUSION

In conclusion, the synthesis of the Eu^{3+} -doped TiO_2 spheres has been performed through mixed-solvent method and the optical properties of the spheres are investigated. The growth conditions of the mixed solvents method were optimized by incorporating ammonia and acetonitrile to obtain monodisperse TiO_2 spheres. The phase transformation condition of the Eu^{3+} -doped TiO_2 spheres was also investigated by

thermal annealing process, in which the amorphous, anatase, and rutile TiO_2 particles were obtained under 350°C , 500°C , and 750°C , respectively. Afterwards, our study also evaluated the optical properties by using PL measurement, which shows the peak emission at 610 nm (red) under the light excitation of 465 nm (blue) and 394 nm (violet) for the Eu^{3+} -doped TiO_2 spheres. The measurement results present that the highest peak red emission can be observed for the anatase phase Eu^{3+} -doped TiO_2 spheres (annealed at 500°C) with low Eu^{3+} molar ratio concentration. Our work also indicates the importance of optimizing the thermal annealing process for different Eu^{3+} molar ratio concentrations of the Eu^{3+} -doped TiO_2 spheres. This study suggested the potential of applying Eu^{3+} -doped TiO_2 spheres as the narrow-line width red phosphor for high efficiency GaN-based white light-emitting diode.

ACKNOWLEDGMENTS

The work was supported by National Nature Science Foundation of China, U.S. Department of Energy (Grant No. NETL, DE-PS26-08NT00290), in part by National Science Foundation (ECCS-1408051, DMR-1505122), and the Daniel E. '39 and Patricia M. Smith Endowed Chair Professorship Fund.

- ¹P. Pust, P. J. Schmidt, and W. Schnick, *Nat. Mater.* **14**, 454–458 (2015).
- ²M. H. Crawford, *IEEE J. Sel. Top. Quantum Electron.* **15**, 1028–1040 (2009).
- ³N. Tansu, H. P. Zhao, G. Y. Liu, X. H. Li, J. Zhang, H. Tong, and Y. K. Ee, *IEEE Photonics J.* **2**, 241–248 (2010).
- ⁴J. Y. Tsao, M. H. Crawford, M. E. Coltrin, A. J. Fischer, D. D. Koleske, G. S. Subramania, G. T. Wang, J. J. Wierer, and R. F. Karlicek, *Adv. Opt. Mater.* **2**, 809 (2014).
- ⁵H. P. Zhao, G. Y. Liu, J. Zhang, J. D. Poplawsky, V. Dierolf, and N. Tansu, *Opt. Express* **19**, A991–A1007 (2011).
- ⁶R. A. Arif, Y. K. Ee, and N. Tansu, *Appl. Phys. Lett.* **91**, 091110 (2007).
- ⁷D. F. Feezell, J. S. Speck, S. P. DenBaars, and S. Nakamura, *J. Disp. Technol.* **9**, 190–198 (2013).
- ⁸C. K. Tan and N. Tansu, *Nat. Nanotechnol.* **10**, 107–109 (2015).
- ⁹R. M. Farrell, E. C. Young, F. Wu, S. P. DenBaars, and J. S. Speck, *Semicond. Sci. Technol.* **27**, 024001 (2012).
- ¹⁰J. Piprek, *Phys. Status Solidi A* **207**, 2217–2225 (2010).
- ¹¹M. F. Schubert, J. Xu, J. K. Kim, E. F. Schubert, M. H. Kim, S. Yoon, S. M. Lee *et al.*, *Appl. Phys. Lett.* **93**, 041102 (2008).
- ¹²H. P. Zhao, G. Y. Liu, J. Zhang, R. A. Arif, and N. Tansu, *J. Disp. Technol.* **9**, 212–225 (2013).
- ¹³Y. C. Shen, G. O. Mueller, S. Watanabe, N. F. Gardner, A. Munkholm, and M. R. Krames, *Appl. Phys. Lett.* **91**, 141101 (2007).
- ¹⁴C. K. Tan and N. Tansu, *AIP Adv.* **5**, 057135 (2015).
- ¹⁵I. E. Titkov, D. A. Sannikov, Y.-M. Park, and J.-K. Son, *AIP Adv.* **2**, 032117 (2012).
- ¹⁶G. Y. Liu, J. Zhang, C. K. Tan, and N. Tansu, *IEEE Photonics J.* **5**, 2201011 (2013).

- ¹⁷T. Fujii, Y. Gao, R. Sharma, E. L. Hu, S. P. DenBaars, and S. Nakamura, *Appl. Phys. Lett.* **84**, 855 (2004).
- ¹⁸J. J. Wierer, A. David, and M. M. Megens, *Nat. Photonics* **3**, 163 (2009).
- ¹⁹J. Jewell, D. Simeonov, S. C. Huang, Y. L. Hu, S. Nakamura, J. Speck, and C. Weisbuch, *Appl. Phys. Lett.* **100**, 171105 (2012).
- ²⁰P. Zhao and H. P. Zhao, *Opt. Express* **20**, A765 (2012).
- ²¹Y. K. Ee, R. A. Arif, N. Tansu, P. Kumnorkaew, and J. F. Gilchrist, *Appl. Phys. Lett.* **91**, 221107 (2007).
- ²²Y. K. Ee, P. Kumnorkaew, R. A. Arif, H. Tong, H. P. Zhao, J. F. Gilchrist, and N. Tansu, *IEEE J. Sel. Top. Quantum Electron.* **15**, 1218–1225 (2009).
- ²³X. H. Li, R. B. Song, Y. K. Ee, P. Kumnorkaew, J. F. Gilchrist, and N. Tansu, *IEEE Photonics J.* **3**, 489–499 (2011).
- ²⁴X. H. Li, P. F. Zhu, G. Y. Liu, J. Zhang, R. B. Song, Y. K. Ee, P. Kumnorkaew, J. F. Gilchrist, and N. Tansu, *J. Disp. Technol.* **9**, 324–332 (2013).
- ²⁵P. Zhu, G. Liu, J. Zhang, and N. Tansu, *J. Disp. Technol.* **9**, 317–323 (2013).
- ²⁶P. F. Zhu and N. Tansu, *Appl. Opt.* **54**, 6305–6312 (2015).
- ²⁷P. F. Zhu, C. K. Tan, W. Sun, and N. Tansu, *Appl. Opt.* **54**, 10299 (2015).
- ²⁸S. Ye, F. Xiao, Y. X. Pan, Y. Y. Ma, and Q. Y. Zhang, *Mater. Sci. Eng., R* **71**, 1–34 (2010).
- ²⁹M. D. McCluskey, L. T. Romano, B. S. Krusor, D. P. Bour, N. M. Johnson, and S. Brennan, *Appl. Phys. Lett.* **72**, 1730–1732 (1998).
- ³⁰H. P. Zhao, G. Y. Liu, and N. Tansu, *Appl. Phys. Lett.* **97**, 131114 (2010).
- ³¹A. Nishikawa, N. Furukawa, T. Kawasaki, Y. Terai, and Y. Fujiwara, *Opt. Mater.* **33**, 1071–1074 (2011).
- ³²J. Hwang, R. Hashimoto, S. Saito, and S. Nunoue, *Appl. Phys. Express* **7**, 071003 (2014).
- ³³R. A. Arif, H. P. Zhao, and N. Tansu, *Appl. Phys. Lett.* **92**, 011104 (2008).
- ³⁴R. Liu, P. Dong, and S.-L. Chen, *Chem. Lett.* **34**, 548–549 (2005).
- ³⁵X. C. Jiang, T. Herricks, and Y. N. Xia, *Adv. Mater.* **15**, 1205–1209 (2003).
- ³⁶M. Pal, J. G. Serrano, P. Santiago, and U. Pal, *J. Phys. Chem. C* **111**, 96–102 (2007).
- ³⁷H. Chu, X. Li, G. Chen, W. Zhou, Y. Zhang, Z. Jin, J. Xu, and Y. Li, *Cryst. Growth Des.* **5**, 1801–1806 (2005).
- ³⁸H.-I. Chen and H.-Y. Chang, *Colloids Surf., A* **242**, 61–69 (2004).
- ³⁹S.-L. Chen, P. Dong, G.-H. Yang, and J.-J. Yang, *Ind. Eng. Chem. Res.* **35**, 4487–4493 (1996).
- ⁴⁰Q. G. Zeng, Z. M. Zhang, Z. J. Ding, Y. Wang, and Y. Q. Sheng, *Scr. Mater.* **57**, 897–900 (2007).
- ⁴¹L. Li, C. K. Tsung, Z. Yang, G. D. Stucky, L. D. Sun, J. F. Wang, and C. H. Yan, *Adv. Mater.* **20**, 903–908 (2008).
- ⁴²K. L. Frindell, M. H. Bartl, A. Popitsch, and G. D. Stucky, *Angew. Chem. - Int. Ed.* **41**, 1001–1004 (2002).
- ⁴³J. G. Li, X. H. Wang, K. Watanabe, and T. Ishigaki, *J. Phys. Chem. B* **110**, 1121–1127 (2006).
- ⁴⁴T. Tsuboi, E. Setiawati, and K. Kawano, *Jpn. J. Appl. Phys., Part 1* **47**, 7428–7435 (2008).
- ⁴⁵J. Ovenstone, P. J. Titler, R. Withnall, and J. Silver, *J. Phys. Chem. B* **105**, 7170–7177 (2001).
- ⁴⁶J. Yang, Z. Quan, D. Kong, X. Liu, and J. Lin, *Cryst. Growth Des.* **7**, 730–735 (2007).
- ⁴⁷R. D. Shannon, *Acta Crystallogr., Sect. A* **32**, 751–767 (1976).
- ⁴⁸T. Tachikawa, T. Ishigaki, J. G. Li, M. Fujitsuka, and T. Majima, *Angew. Chem. - Int. Ed.* **120**, 5428–5432 (2008).
- ⁴⁹Q. G. Zeng, Z. J. Ding, and Z. M. Zhang, *J. Lumin.* **118**, 301–307 (2006).